Storage-constrained dispatch and exergy analysis of a grid-connected solar photovoltaic–reversible solid oxide cell–metal hydride hydrogen storage microgrid

Alexandros Arsalis[a,b], Pavlos Papadopoulos[a,c,d], Aravind Purushothaman Vellayani[d] and George E. Georghiou[a,b]

[a] *PHAETHON Centre of Excellence for Intelligent, Efficient and Sustainable Energy Solutions, Nicosia, Cyprus, arsalis@ucy.ac.cy, CA, papadopoulos.pavlos@ucy.ac.cy, geg@ucy.ac.cy*
[b] *PV Technology Laboratory, Department of Electrical and Computer Engineering, Nicosia, Cyprus*
[c] *Department of Mechanical and Manufacturing Engineering, Nicosia, Cyprus*
[d] *Energy Conversion Group, Energy and Sustainability Research Institute Groningen, Faculty of Science and Engineering, University of Groningen, The Netherlands, a.purushothaman.vellayani@rug.nl*

Abstract:

In the pursuit of sustainable decentralized energy systems, the integration of renewable generation with long-duration storage is essential. This study presents an hourly system-level simulation of a grid-connected photovoltaic (PV)–reversible solid oxide cell (rSOC)–metal hydride (MH) microgrid, with emphasis on storage-constrained dispatch and integrated energy management. The model is implemented in Engineering Equation Solver (EES) with hourly resolution over an annual horizon and captures the coupled electrical, hydrogen, and thermal interactions. Unlike conventional approaches, the proposed dispatch explicitly enforces hydrogen storage feasibility at each time step, ensuring physically consistent system operation. Results show that PV generation supplies approximately 40% of the annual load, while grid imports account for about 60%, indicating partial grid dependency. Hydrogen production and consumption remain balanced (17,454 kg annually), confirming stable cyclic operation of the storage subsystem. The rSOC enables bidirectional energy conversion and temporal shifting of renewable energy. Exergy analysis reveals that the dominant source of irreversibility is the PV subsystem (56.2%), followed by rSOC electrochemical processes and power electronics, while hydrogen storage contributes marginally. The results demonstrate that storage-constrained dispatch ensures realistic operation and that improvements in PV conversion efficiency and rSOC performance are critical for enhancing overall system efficiency.

Keywords:

Exergy; Green hydrogen; Microgrid; Reversible solid oxide cell; Sustainability.

1. Introduction

The transition toward low-carbon energy systems has become a central priority in response to climate change, increasing energy demand, and concerns over energy security. Renewable energy sources (RES), particularly solar photovoltaic (PV) systems, play a key role due to their scalability, cost competitiveness, and environmental benefits. However, the inherent intermittency and variability of PV generation introduce challenges for power system stability and reliability, especially at high penetration levels. Microgrids provide an effective solution by enabling localized energy management, improving resilience, and facilitating the integration of distributed energy resources [1]. In this context, energy storage technologies are essential for balancing supply and demand. Battery energy storage systems (BESS) offer high-efficiency, short-term flexibility, while hydrogen-based systems provide long-duration and seasonal storage capabilities [2]. Green hydrogen, produced via water electrolysis using renewable electricity, is increasingly recognized as a promising energy carrier for decarbonizing multiple sectors, including power, transport, and industry [3].

Recent research has focused on hybrid PV–hydrogen microgrids, which integrate PV generation with electrolyzers, hydrogen storage systems, and fuel cells [4]. These systems enable the conversion of excess renewable electricity into hydrogen during periods of surplus generation and its reconversion into electricity during periods of deficit [5]. Several studies have demonstrated that such hybrid systems can enhance energy autonomy, improve reliability, and reduce dependence on external grid supply [6]. In particular, advanced control and optimization strategies have been proposed to coordinate PV generation, hydrogen production,

and storage utilization under varying operating conditions [7]. Furthermore, hybrid renewable microgrids combining PV, batteries, and hydrogen storage have shown improved operational performance through optimal sizing and coordinated dispatch of system components [8]. These studies highlight the importance of integrating multiple storage technologies to address both short-term and long-term variability in renewable generation [9]. At the same time, recent works emphasize the need for more detailed modeling approaches that capture the interactions between electrical, hydrogen, and thermal subsystems, as well as the dynamic behavior of electrochemical conversion devices [10].

Despite these advances, several research gaps remain [11]. First, many existing studies adopt simplified representations of electrolyzers and fuel cells, often assuming constant efficiencies that do not reflect realistic operating conditions. Second, the coupling between electrical, hydrogen, and thermal domains is frequently oversimplified, limiting the ability to assess integrated system performance. Third, dispatch strategies in hybrid PV–hydrogen systems are typically neglecting strict enforcement of hydrogen storage constraints, leading to potentially infeasible operation near storage limits. Recent studies have specifically investigated the integration and operation of reversible solid oxide cell (rSOC) systems within renewable-based microgrids. Huang et al. [12] analyzed the optimal operation of rSOC systems considering heat recovery and mode-switching dynamics, highlighting the importance of thermal integration and operational flexibility. Similarly, Liu et al. [13] evaluated the efficiency performance of rSOC systems under different thermal configurations, demonstrating the strong influence of heat recovery on system efficiency. In addition, advanced control strategies for rSOC operation in microgrids have been proposed, focusing on predictive control and mode-switching behavior [14,15].

However, these approaches typically do not explicitly enforce storage-feasible dispatch under hydrogen inventory constraints. Motivated by these gaps, this study develops a comprehensive system-level model of a grid-connected PV–rSOC–metal hydride microgrid. The objective is to investigate the optimal coupling between PV generation and rSOC operation, considering hydrogen storage constraints and system-level efficiency. To the best of the authors' knowledge, no prior study combines storage-feasible dispatch with integrated PV–rSOC–metal hydride systems while explicitly enforcing hydrogen inventory constraints at each time step. The remainder of this paper is organized as follows. Section 2 presents the system configuration and modeling methodology. Section 3 discusses the results and system performance. Section 4 concludes the study and outlines future work.

2. Material and methods

2.1. System design and configuration

Figure 1 illustrates the grid-connected PV–rSOC–metal hydride (MH) campus microgrid, including electrical, hydrogen, and thermal couplings. Electricity generated by the PV system is supplied to the campus AC bus and distributed to local loads, exported to the grid, or directed to the bidirectional rSOC interface. Hydrogen is exchanged between the rSOC stack and the MH storage tank through a hydrogen manifold, enabling long-duration energy storage. Thermal energy recovered from the rSOC is utilized for steam generation and MH heating, while system operation is coordinated by a supervisory controller based on real-time sensor inputs. The system boundary includes PV generation, power electronics, the rSOC unit, MH hydrogen storage, campus electrical loads, thermal recovery components, and grid import/export. Hydrogen is assumed to be produced, stored, and consumed entirely within the system boundary.

The system is modeled as a grid-connected campus microgrid operating under hourly resolution, where each timestep represents quasi-steady-state electrical and electrochemical behavior. The PV subsystem is described using a temperature-dependent efficiency with constant power electronics efficiencies. The rSOC operates in both electrolysis (SOEC) and fuel cell (SOFC) modes using a reduced-order representation, while degradation effects are neglected. Hydrogen storage is modeled as a lumped system with fixed capacity limits, and charging/discharging is constrained by storage availability. A supervisory control strategy governs system operation based on PV surplus or deficit and hydrogen inventory, explicitly enforcing storage feasibility at each time step. Thermal integration is represented through simplified heat recovery from the rSOC to the steam generation and MH subsystems. Electricity is treated as pure exergy, with the reference environment defined by ambient conditions. All components are assumed to operate with constant performance over the simulation horizon.

2.2. Modeling methodology

2.2.1. Overall microgrid model

The investigated system is modeled as a grid-connected hybrid microgrid integrating PV generation, an rSOC unit operating in both SOEC and SOFC modes, and an MH hydrogen storage subsystem. The system is simulated using an hourly time resolution over an annual horizon, where each time step is treated as quasi-steady with respect to electrical and electrochemical processes, while capturing the dynamic evolution of hydrogen storage.

At the system level, microgrid operation is governed by coupled electrical and hydrogen energy balances. The instantaneous electrical balance is defined at the campus AC bus as:

$$P_{PV,AC} + P_{rSOC,AC}^{out} + P_{grid,import} = P_{load,AC} + P_{rSOC,AC}^{in} + P_{grid,export} \quad (1)$$

where $P_{PV,AC}$ is the AC power generated by the PV system, $P_{load,AC}$ is the campus electrical demand, $P_{rSOC,AC}^{in}$ and $P_{rSOC,AC}^{out}$ represent the electrical power consumed and produced by the rSOC in SOEC and SOFC modes, respectively, and $P_{grid,import}$ and $P_{grid,export}$ denote power exchanged with the utility grid.

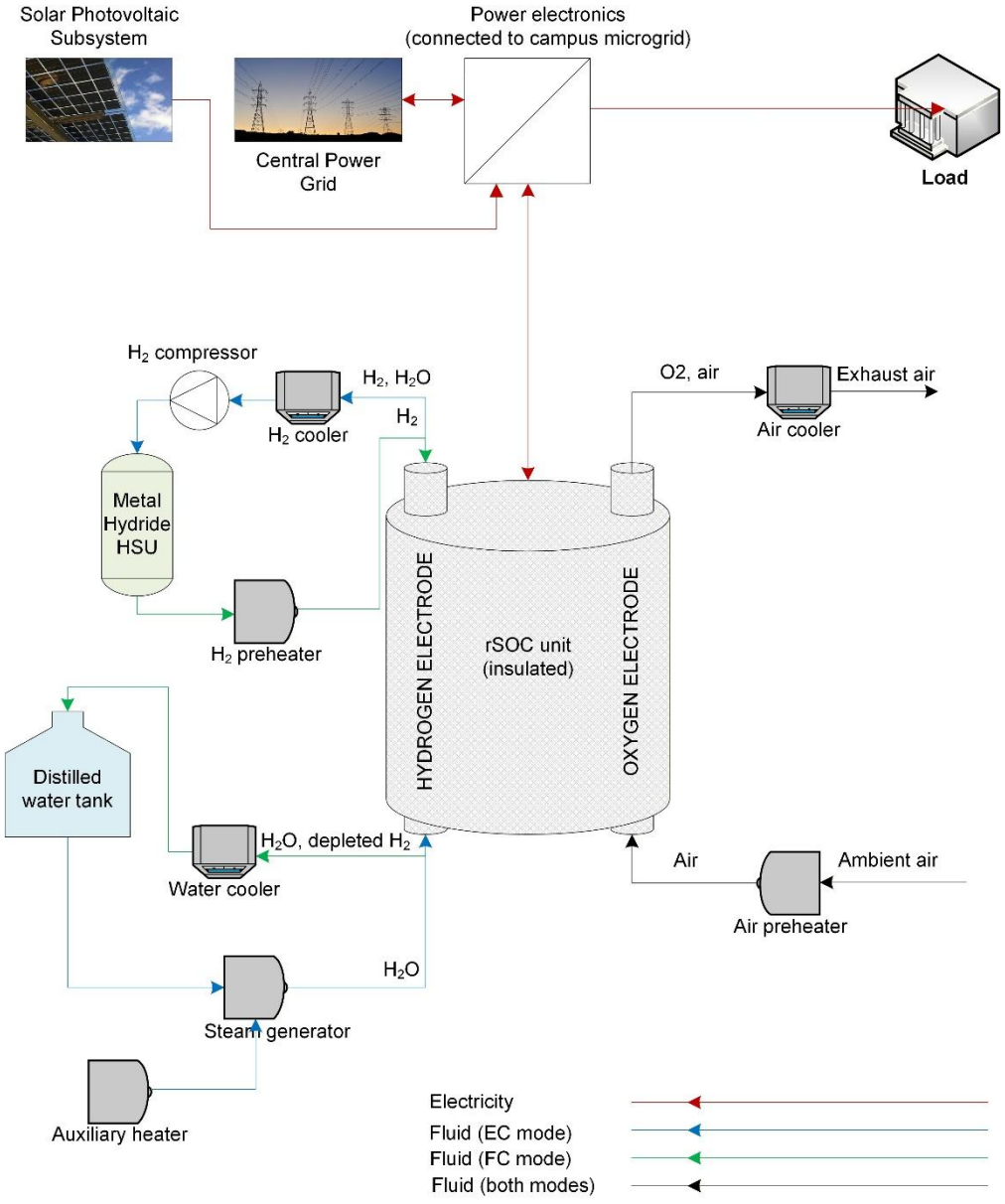

Figure 1. *Integrated schematic of the grid-connected PV–rSOC–MH campus energy system showing electrical, hydrogen, and thermal couplings.*

Hydrogen acts as an intermediate energy carrier enabling long-duration storage. The hydrogen inventory in the MH tank is updated at each time step according to:

$$H2_{tank}(t+1) = H2_{tank}(t) + \dot{m}_{H2}^{prod}\,\Delta t - \dot{m}_{H2}^{cons}\,\Delta t \quad (2)$$

where $\dot{m}_{H2}^{prod}$ and $\dot{m}_{H2}^{cons}$ are the hydrogen production and consumption rates associated with SOEC and SOFC operation, respectively, and Δt is the simulation time step.

The system operation is governed by a supervisory dispatch strategy based on the instantaneous PV power surplus or deficit, defined as:

$$P_{surplus} = P_{PV,AC} - P_{load,AC} \quad (3)$$

When $P_{surplus} > 0$, the rSOC operates in SOEC mode to convert excess electricity into hydrogen, subject to storage capacity constraints. Conversely, when $P_{surplus} < 0$ and sufficient hydrogen is available, the rSOC operates in SOFC mode to supply electricity to the load. Importantly, the dispatch is constrained by hydrogen storage feasibility, ensuring that hydrogen production and consumption within each time step do not violate the physical limits of the MH tank.

The main system state variables are the hydrogen inventory $H2_{tank}$ and the rSOC operating mode, which together determine the system dynamics and energy flows. Thermal interactions between subsystems are represented in a simplified manner through heat recovery from the rSOC unit, which is utilized for steam generation and hydrogen desorption processes.

2.2.2. Photovoltaic generation model

The PV subsystem converts incident solar irradiance into electrical power, which is supplied to the campus AC bus after power conditioning. The PV output is modeled using a temperature-dependent efficiency formulation, accounting for the influence of cell temperature on conversion performance.

The instantaneous electrical efficiency of the PV modules is expressed as:

$$\eta_{PV} = \eta_{PV,ref}\left[1-\beta_{PV}\left(T_{PV}-T_{ref}\right)\right] \quad (4)$$

where $\eta_{PV,ref}$ is the reference efficiency at the reference temperature T_{ref}, β_{PV} is the temperature coefficient, and T_{PV} is the PV cell temperature.

The solar power incident on the PV array is given by:

$$P_{solar} = A_{PV} \cdot G \quad (5)$$

where A_{PV} is the total PV array area and G is the global solar irradiance.

The DC electrical power generated by the PV system is then calculated as:

$$P_{PV,DC} = \eta_{PV} \cdot P_{solar} \quad (6)$$

To account for power electronics, constant efficiency is assumed for the DC/DC converter and inverter stages. The maximum available AC power from the PV system is therefore expressed as:

$$P_{PV,AC} = \eta_{DC/DC} \cdot \eta_{INV} \cdot P_{PV,DC} \quad (7)$$

where $\eta_{DC/DC}$ and η_{INV} represent the efficiencies of the DC/DC converter and inverter, respectively.

The PV system operates under maximum power point tracking (MPPT), ensuring that the available solar power is fully utilized at each time step.

Curtailment is implicitly captured at the system level when PV generation exceeds the combined demand of the load and the storage-constrained rSOC operation.

2.2.3. Reversible solid oxide cell model

The rSOC unit operates in two modes: SOEC for hydrogen production and SOFC for electricity generation. A reduced-order electrochemical model is employed to capture the main performance characteristics while maintaining computational efficiency.

The cell voltage is expressed as the sum of reversible voltage and polarization losses:

$$V_{cell} = V_{rev} \pm \eta_{act} \pm \eta_{ohm} \pm \eta_{conc} \quad (8)$$

where the positive sign applies to SOEC operation and the negative sign to SOFC operation.

The reversible voltage is determined using a Nernst-type expression:

$$V_{rev} = E^0 + \frac{RT}{2F}\ln\left(\frac{p_{H_2} \cdot p_{O_2}^{1/2}}{p_{H_2O}}\right) \quad (9)$$

Activation losses are described using a simplified Butler–Volmer formulation:

$$\eta_{act} = \frac{RT}{\alpha 2F}\ln\left(1+\frac{j}{j_0}\right) \quad (10)$$

Ohmic losses are calculated as:

$$\eta_{ohm} = j \cdot ASR \quad (11)$$

where j is the current density and ASR is the area-specific resistance.

The stack power is given by:

$$P_{stack} = \frac{N_{cells} \cdot V_{cell} \cdot I}{1000} \quad (12)$$

where N_{cells} is the number of cells and I is the stack current.

Hydrogen production and consumption are derived from Faraday's law:

$$\dot{n}_{H_2} = \frac{N_{cells} \cdot I}{2F} \quad (13)$$

For SOEC operation, hydrogen is produced and stored, whereas for SOFC operation, hydrogen is consumed to generate electricity. Mode-dependent efficiencies are incorporated through power electronics and auxiliary consumption, which are accounted for in the overall system energy balance.

The electrical interaction between the rSOC stack and the AC microgrid is modeled through power electronics and auxiliary components, which introduce additional losses and determine the net power exchanged with the campus AC bus. The rSOC operates under commanded power setpoints, defined as $P_{SOEC,cmd}$ and $P_{SOFC,cmd}$, corresponding to electrolysis and fuel cell operation, respectively.

In SOEC mode, electrical power is drawn from the AC bus and converted to DC power supplied to the stack:

$$P_{rSOC,AC}^{in} = \frac{P_{stack}^{SOEC}}{\eta_{PE} \cdot \eta_{aux}} \quad (14)$$

where η_{PE} represents the power electronics efficiency and η_{aux} accounts for auxiliary consumption (e.g., pumps, blowers, and control systems).

In SOFC mode, the stack produces DC electrical power, which is converted to AC and delivered to the campus bus:

$$P_{rSOC,AC}^{out} = P_{stack}^{SOFC} \cdot \eta_{PE} \cdot \eta_{INV} \cdot \eta_{aux} \quad (15)$$

where $\eta_{INV}$is the inverter efficiency.

The commanded powers are constrained by the nominal rSOC capacity:

$$0 \le P_{SOEC,cmd} \le P_{rSOC,max}, 0 \le P_{SOFC,cmd} \le P_{rSOC,max} \quad (16)$$

These commands are determined by the supervisory dispatch strategy and further limited by hydrogen storage feasibility, ensuring physically consistent operation. The electrical efficiency of the rSOC system can be expressed in a mode-dependent manner. In SOEC mode, the effective conversion efficiency is defined as the ratio of the chemical energy stored in hydrogen to the electrical energy consumed:

$$\eta_{SOEC} = \frac{\dot{m}_{H_2}^{prod} \cdot LHV_{H_2}}{P_{rSOC,AC}^{in}} \quad (17)$$

In SOFC mode, the efficiency is defined as the ratio of electrical output to the chemical energy input from hydrogen:

$$\eta_{SOFC} = \frac{P_{rSOC,AC}^{out}}{\dot{m}_{H_2}^{cons} \cdot LHV_{H_2}} \quad (18)$$

Additionally, a fraction of the thermal energy generated by the rSOC is assumed to be recoverable:

$$Q_{rec} = f_{rec} \cdot Q_{rSOC} \quad (19)$$

where f_{rec} is the heat recovery factor. This recovered heat is utilized for steam generation in SOEC mode and hydrogen desorption in the MH storage subsystem.

2.2.4. Metal hydride hydrogen storage model

The hydrogen storage subsystem is modeled using a lumped MH tank, which enables reversible hydrogen absorption and desorption coupled with thermal effects.

At the system level, storage is represented through a mass balance on the stored hydrogen inventory, which acts as a key state variable governing system operation. The storage system is constrained by minimum and maximum capacity limits:

$$H2_{tank,min} \leq H2_{tank}(t) \leq H2_{tank,max} \quad (20)$$

These bounds ensure safe and physically feasible operation and are explicitly enforced within the dispatch control strategy. The MH tank operates through thermally coupled absorption and desorption processes. During SOEC operation, hydrogen is stored via an exothermic absorption process, requiring heat removal from the MH bed. Conversely, during SOFC operation, hydrogen is released through an endothermic desorption process, requiring heat input. These thermal interactions are represented in a simplified manner through heat exchange with the rSOC heat recovery system.

The effective hydrogen charging and discharging rates are therefore not only determined by the electrochemical production and consumption rates but also by the available storage capacity and thermal conditions. In the present model, a reduced-order approach is adopted, where detailed kinetics and pressure-dependent equilibrium behavior are not explicitly resolved, and the storage system is treated as a capacity-limited buffer with thermally assisted operation.

2.2.5. Dispatch control strategy

The operation of the microgrid is governed by a supervisory dispatch control strategy that determines the operating mode and power setpoints of the rSOC unit based on the instantaneous balance between PV generation, load demand, and hydrogen storage availability. The control decision is based on the PV power surplus or deficit, defined as:

$$P_{surplus} = P_{PV,AC} - P_{load,AC} \quad (21)$$

When $P_{surplus} > 0$, excess PV generation is available and the rSOC is operated in SOEC mode to convert surplus electricity into hydrogen. Conversely, when $P_{surplus} < 0$, a power deficit exists and the rSOC operates in SOFC mode to generate electricity, provided that sufficient hydrogen is available in the storage tank. If neither condition is satisfied, the rSOC remains idle.

The operating mode is therefore determined as:

$$\text{Mode} = \begin{cases} \text{SOEC}, & P_{surplus} > 0 \text{ and } H2_{tank} < H2_{tank,max} \\ \text{SOFC}, & P_{surplus} < 0 \text{ and } H2_{tank} > H2_{tank,min} \\ \text{Idle}, & \text{otherwise} \end{cases} \quad (22)$$

The commanded power of the rSOC is initially determined by the magnitude of the surplus or deficit and is limited by the nominal rSOC capacity:

$$P_{SOEC,cmd}^{raw} = \min\left(P_{surplus}, P_{rSOC,max}\right) \quad (23)$$

$$P_{SOFC,cmd}^{raw} = \min\left(|P_{surplus}|, P_{rSOC,max}\right) \quad (24)$$

To ensure physically consistent operation, the commanded powers are further constrained by hydrogen storage feasibility. Specifically, hydrogen production and consumption within each time step must not exceed the available storage capacity or the available hydrogen inventory.

This is enforced through feasibility factors derived from the remaining storage capacity and available hydrogen:

$$f_{SOEC} = \min\left(1, \frac{H2_{tank,max} - H2_{tank}}{\dot{m}_{H_2}^{prod,raw}\,\Delta t}\right) \quad (25)$$

$$f_{SOFC} = \min\left(1, \frac{H2_{tank} - H2_{tank,min}}{\dot{m}_{H_2}^{cons,raw}\,\Delta t}\right) \quad (26)$$

The final commanded powers are therefore:

$$P_{SOEC,cmd} = f_{SOEC} \cdot P_{SOEC,cmd}^{raw} \quad (27)$$

$$P_{SOFC,cmd} = f_{SOFC} \cdot P_{SOFC,cmd}^{raw} \quad (28)$$

This formulation ensures intra-timestep feasibility by explicitly enforcing hydrogen storage constraints, avoiding the infeasible operation often encountered in conventional dispatch strategies. Hydrogen production and consumption are therefore always consistent with storage limits, preventing overfilling or depletion of the MH tank within a single time step. The dispatch prioritizes direct use of PV generation to meet the load, followed

by hydrogen production during surplus periods and electricity generation from stored hydrogen during deficit periods. This hierarchical approach enables efficient renewable energy utilization while maintaining physically consistent and stable system operation.

2.2.6. Grid interaction

The microgrid is connected to the utility grid through a bidirectional interface, enabling electricity import and export depending on the instantaneous balance between local generation and demand. The grid acts as a balancing mechanism to ensure that the electrical demand is always satisfied when local resources are insufficient and to absorb excess generation when surplus energy cannot be utilized or stored.

At each time step, the net power balance at the campus AC bus is evaluated as:

$$P_{net} = P_{PV,AC} + P_{rSOC,AC}^{out} - P_{load,AC} - P_{rSOC,AC}^{in} \quad (29)$$

Based on this balance, grid exchange is determined as:

$$P_{grid,export} = \max(0, P_{net}) \quad (30)$$

$$P_{grid,import} = \max(0, -P_{net}) \quad (31)$$

where $P_{grid,export}$ represents electricity exported to the grid and $P_{grid,import}$ represents electricity imported from the grid.

The grid is assumed to have sufficient capacity to accommodate all power exchanges, with no explicit limits imposed on import or export. It is therefore modeled as an infinite source and sink of electricity, providing flexibility to balance short-term mismatches between generation and demand. Grid interaction ensures supply continuity during periods of low PV generation and limited hydrogen availability, while excess PV generation is exported when it cannot be utilized by the load or stored via the rSOC. This approach enables the quantification of grid dependency through cumulative indicators, such as total annual grid import and export.

2.2.7. Thermal integration

Thermal interactions within the microgrid are primarily associated with the operation of the rSOC unit and the MH hydrogen storage subsystem. Due to the high operating temperature of the rSOC, a significant amount of thermal energy is generated during both SOEC and SOFC operation. This thermal energy can be partially recovered and utilized within the system to improve overall efficiency. In the present model, a simplified thermal integration approach is adopted, where a fraction of the rSOC thermal output is considered recoverable and redistributed to support auxiliary thermal demands.

The recoverable heat is expressed as:

$$Q_{rec} = f_{rec} \cdot Q_{rSOC} \quad (32)$$

where Q_{rSOC} represents the total thermal energy generated by the rSOC and f_{rec} is the heat recovery factor.

The recovered heat is primarily utilized for two purposes. First, in SOEC mode, it is used to support steam generation, reducing the external energy required for water evaporation and superheating. Second, in SOFC mode, it is directed to the MH storage subsystem to provide the heat required for hydrogen desorption, which is an endothermic process. The thermal demand associated with the MH unit is represented in a simplified manner, where heat is required during hydrogen release and removed during hydrogen absorption. The interaction between the rSOC and MH subsystems therefore creates a thermally coupled system, in which recovered heat enhances storage performance and reduces auxiliary energy requirements.

Any excess thermal energy that cannot be utilized within the system is assumed to be rejected to the environment. Detailed spatial temperature gradients, heat exchanger dynamics, and transient thermal behavior are not explicitly modeled; instead, a lumped representation is adopted to maintain computational efficiency. This simplified thermal integration framework captures the key role of heat recovery in improving system performance, while remaining consistent with the system-level modeling approach and the focus on energy and exergy analysis. Detailed thermal dynamics are not modeled to maintain computational efficiency at the system level.

2.2.8. Exergy analysis

An exergy analysis is performed to evaluate the thermodynamic performance of the integrated microgrid and to identify the main sources of irreversibility within the system. The analysis is conducted at the system level, considering the major energy flows associated with PV generation, grid interaction, rSOC operation, and hydrogen storage. Electricity is treated as pure exergy, such that electrical power is directly equivalent to exergy flow.

The chemical exergy of hydrogen is approximated using its lower heating value (LHV), which provides a suitable estimate for system-level analysis:

$$Ex_{H_2} = \dot{m}_{H_2} \cdot LHV_{H_2} \quad (33)$$

Thermal exergy associated with recovered heat is evaluated using the Carnot factor:

$$Ex_Q = Q\left(1-\frac{T_0}{T}\right) \quad (34)$$

where Q is the heat flow, T is the temperature at which heat is available, and T_0 is the ambient reference temperature.

The reference environment for the exergy analysis is defined by an ambient temperature of $T_0 = 298.15$ K and a reference pressure of $P_0 = 1$ atm. These conditions are used to evaluate the exergy content of thermal and chemical energy flows consistently across all system components.

The total exergy input to the system at each time step is defined as:

$$Ex_{in} = Ex_{PV} + Ex_{grid,import} \quad (35)$$

where Ex_{PV} represents the exergy associated with PV-generated electricity and $Ex_{grid,import}$ corresponds to imported electrical energy.

The useful exergy output is defined as:

$$Ex_{out} = Ex_{load,served} + Ex_{grid,export} + \Delta Ex_{H_2} \quad (36)$$

where $Ex_{load,served}$ is the exergy delivered to the campus load, $Ex_{grid,export}$ is the exergy exported to the grid, and ΔEx_{H_2} represents the net change in stored hydrogen exergy.

The exergy destruction within the system is then obtained from the exergy balance:

$$Ex_{dest} = Ex_{in} - Ex_{out} \quad (37)$$

The overall system exergy efficiency is defined as:

$$\eta_{ex} = \frac{Ex_{out}}{Ex_{in}} \quad (38)$$

This approach enables the quantification of thermodynamic losses associated with each subsystem, including PV conversion, electrochemical processes in the rSOC, hydrogen storage, and power electronics. By evaluating exergy destruction, the analysis provides insights into the dominant sources of inefficiency and supports the identification of opportunities for system improvement and optimization. The exergy metrics are aggregated over the annual simulation period to assess the overall thermodynamic performance of the microgrid under realistic operating conditions.

2.2.9. Simulation framework and performance indicators

The developed model is implemented in Engineering Equation Solver (EES) using a parametric table approach and executed with hourly resolution over an annual horizon (8760 time steps). Each time step represents quasi-steady system operation, while key state variables, particularly the hydrogen inventory in the MH tank, are updated sequentially to capture system dynamics.

At each step, the model evaluates PV generation, load demand, rSOC operation, hydrogen production or consumption, and grid interaction, ensuring consistency with the storage-constrained dispatch strategy. Time-series inputs, including solar irradiance, ambient temperature, and load demand, are provided as hourly datasets and processed sequentially.

Energy-based metrics include total PV generation E_{PV}, total grid import $E_{grid,import}$, total grid export $E_{grid,export}$, and total hydrogen production and consumption, obtained by summing hourly values over the year. System efficiency is defined as the ratio of useful energy delivered to the load to the total energy input from PV and grid sources. Grid dependency and self-sufficiency are quantified based on the relative contributions of local generation and grid imports.

Operational indicators, including the number of hours in SOEC, SOFC, and idle modes, as well as the evolution of hydrogen storage levels, provide additional insight into system utilization and dispatch effectiveness. Together with exergy-based metrics, these indicators enable a comprehensive evaluation of system performance and support the analysis presented in the Results and Discussion section.

3. Results and discussion

3.1. System operation and energy flows

The operation of the proposed microgrid is governed by the balance between PV generation and campus electrical demand, as well as the availability of hydrogen storage. Figure 2 illustrates the temporal evolution of PV generation, load demand, and rSOC operation over a year. The results show that the supervisory dispatch strategy effectively coordinates system operation based on the instantaneous power surplus or deficit. During periods of high solar irradiance, when $P_{PV,AC} > P_{load,AC}$, excess PV generation is directed to the rSOC operating in SOEC mode, enabling the conversion of surplus electricity into hydrogen. The electrolysis power follows the available surplus when feasible, while remaining constrained by the nominal rSOC capacity and hydrogen storage limits. Conversely, during periods of low PV generation or high demand, when $P_{PV,AC} < P_{load,AC}$, the rSOC operates in SOFC mode, supplying electricity to the campus by converting stored hydrogen, subject to storage availability. This bidirectional operation enables energy shifting across time, while periods of insufficient hydrogen or limited capacity are compensated through grid imports.

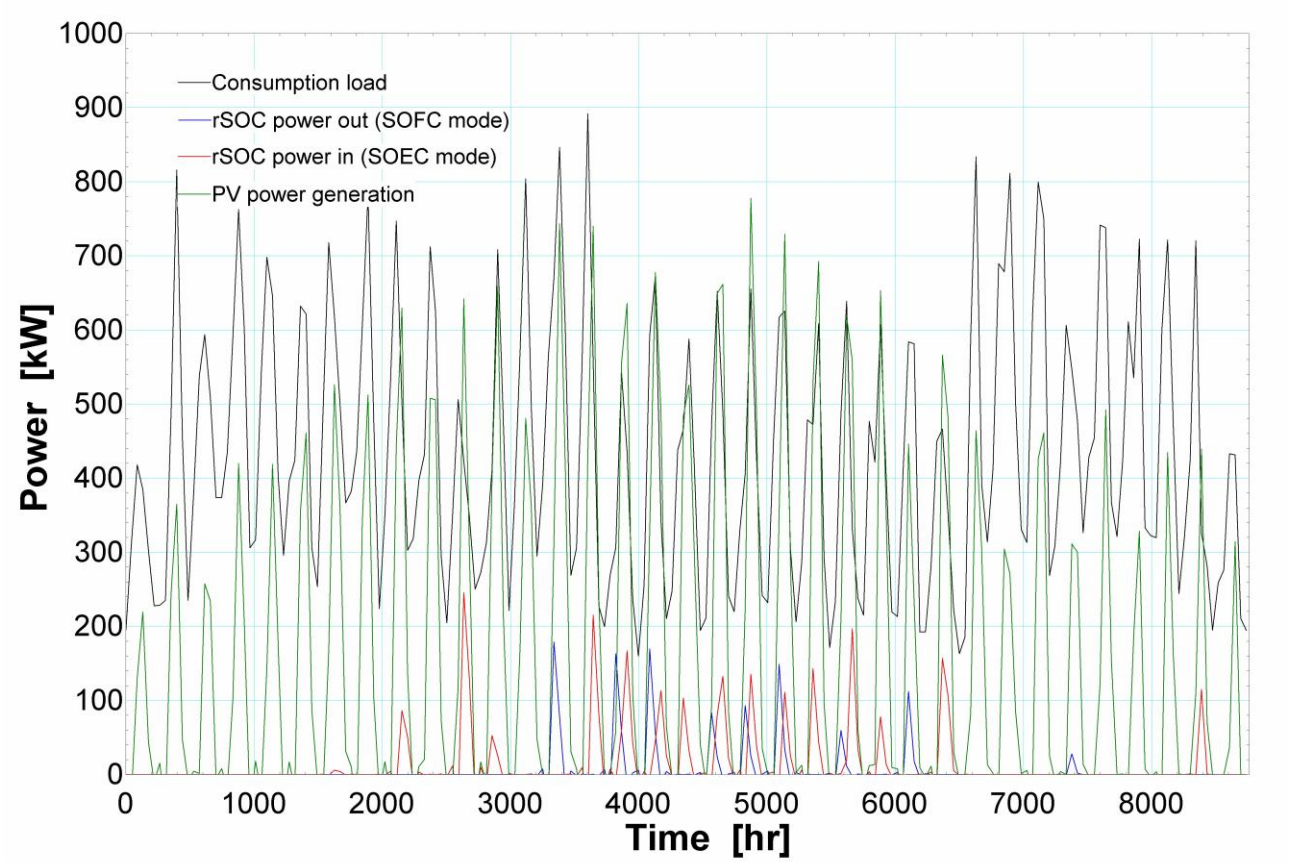

Figure 2. *Hourly profiles of PV generation, load demand, and rSOC operation over the annual simulation.*

The evolution of the hydrogen storage level, shown in Figure 3, reflects the interaction between PV availability and system demand. The hydrogen tank is charged during periods of excess PV generation and discharged during deficit periods, exhibiting both short-term cycling and longer-term variations driven by seasonal imbalances between generation and demand. Importantly, the storage-constrained dispatch ensures that the hydrogen inventory remains within the defined bounds at all times, preventing overfilling and depletion within individual time steps. The rSOC operates in SOEC, SOFC, and idle modes for approximately 11.5%, 6.6%, and 81.9% of the annual operation, respectively.

Grid interaction occurs during periods when local PV generation and available hydrogen storage are insufficient to meet the load demand. In such cases, electricity is imported from the grid to ensure supply continuity. Conversely, grid export occurs when PV generation exceeds both the load demand and the storage-constrained rSOC charging capacity. The results highlight the complementary role of the grid in balancing residual mismatches, while the coordinated operation of PV generation, rSOC conversion, and hydrogen storage enables effective energy management under physically constrained operation.

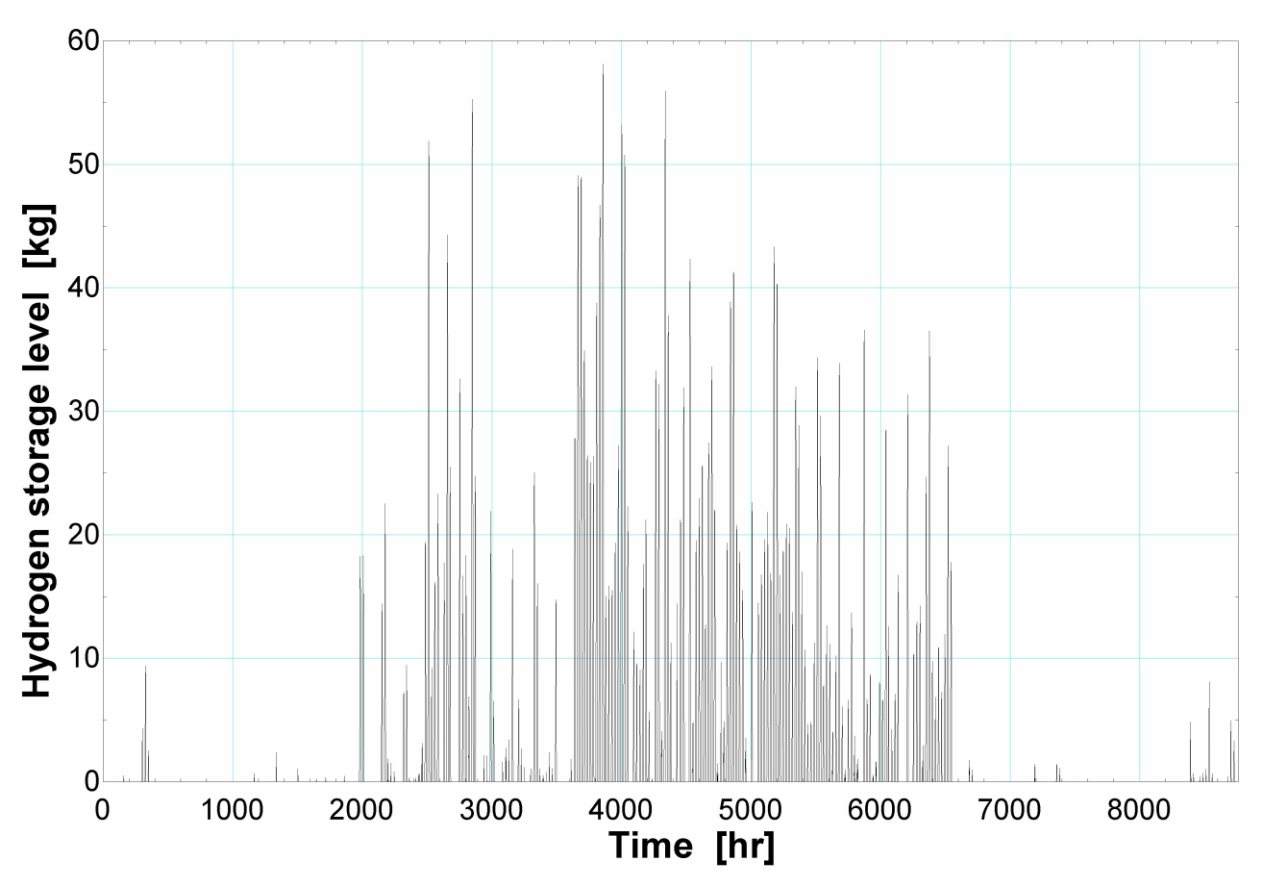

Figure 3. *Hourly evolution of hydrogen storage level over the annual simulation.*

3.2. System performance and efficiency

Table 1 presents the main system capacities considered in this study. The PV system is sized at 847.4 kW, providing the primary renewable energy input to the microgrid. The rSOC unit operates with a nearly symmetric capacity in both modes, with a maximum input of 398.9 kW in SOEC mode and a maximum output of 400 kW in SOFC mode, enabling bidirectional energy conversion between electricity and hydrogen. The MH hydrogen storage capacity of 58 kg defines the upper limit for hydrogen buffering and plays a critical role in determining the system's ability to shift energy across time. The selected capacities reflect a design trade-off between renewable utilization, storage capability, and system flexibility.

Table 1. *Capacities of the main system units of the proposed microgrid system.*

Parameter	Value	Unit
PV maximum power output	847.4	kW
rSOC maximum power input (SOEC mode)	398.9	kW
rSOC maximum power output (SOFC mode)	400	kW
Metal hydride hydrogen storage capacity	58	kg

The overall performance of the proposed microgrid is evaluated using aggregated annual energy and exergy indicators. Table 2 summarizes the main energy flows, including total PV generation (E_{PV}), grid import $(E_{grid,import})$, grid export $(E_{grid,export})$, as well as total hydrogen production and consumption. The results show that the total annual load demand is 3811 MWh, while PV generation accounts for 1526 MWh, corresponding to approximately 40% of the demand. The remaining demand is primarily covered by grid imports (2336 MWh), indicating a significant grid dependency (~60%). Grid exports are negligible, as excess PV generation is preferentially utilized for hydrogen production within the limits imposed by the storage-constrained dispatch strategy.

The total hydrogen production and consumption are equal (17,454 kg), confirming cyclic operation of the storage system over the annual horizon. Hydrogen is produced during periods of surplus PV generation and consumed during deficit periods, enabling temporal decoupling between energy supply and demand. The

integration of the rSOC and MH storage enhances system flexibility by facilitating energy shifting across time and reducing grid imports, particularly during periods of low solar availability.

Table 2. *Performance summary of the proposed microgrid system.*

Parameter	Value	Unit
Total annual consumption load	3811	MWh
Total annual PV generation	1526	MWh
Total annual grid imports	2336	MWh
Total annual grid exports	~0	MWh
Total hydrogen production	17454	kg
Total hydrogen consumption	17454	kg

However, grid dependency is not fully eliminated, as extended periods of low PV generation and limited hydrogen availability still require external electricity supply. The results reflect the combined impact of PV conversion losses, power electronics inefficiencies, and electrochemical losses within the rSOC unit. The obtained PV contribution and grid dependency are consistent with reported values in similar PV–hydrogen microgrid studies, where PV shares typically range between 30–60% depending on system sizing and storage capacity.

3.3. Exergy-based performance assessment

Exergy analysis is used to identify the components that most strongly limit the thermodynamic performance of the microgrid and to assess where system improvements would be most effective. The results indicate that the dominant source of exergy destruction is the PV subsystem (56.2%), followed by the rSOC during SOEC (11.2%) and SOFC (11.1%) operation. Additional losses arise from power electronics in SOEC (9.2%) and SOFC (7.7%) modes, while the contribution of the MH storage is relatively small, with absorption and desorption accounting for 2.6% and 2.2%, respectively.

These results provide key insights into system design and operational performance. The dominance of PV-related exergy destruction indicates that overall system performance is primarily constrained at the energy generation stage rather than within the storage subsystem. This implies that improvements in PV conversion efficiency, thermal management, or hybridization with other renewable sources would yield greater system-level benefits than further refinement of hydrogen storage. Moreover, the combined contribution of rSOC electrochemical and power electronic losses (~39%) highlights the importance of accurately representing conversion efficiencies and operational behavior. In this context, the use of a storage-constrained dispatch becomes particularly relevant, as it ensures that rSOC operation occurs only when it is thermodynamically and physically justified, avoiding unrealistic cycling that would artificially increase exergy losses. Additionally, the relatively small exergy destruction associated with the MH storage subsystem confirms that hydrogen storage acts primarily as an energy buffer rather than a major source of inefficiency. This supports the suitability of MH storage for long-duration applications, where its thermodynamic penalties remain limited compared to conversion processes.

Finally, the exergy results provide guidance for future system optimization. Specifically, they indicate that performance improvements should focus on (a) enhancing PV conversion efficiency, (b) reducing rSOC overpotentials and auxiliary consumption, and (c) improving power electronics efficiency. In contrast, further optimization of storage thermodynamics is expected to yield only marginal gains at the system level.

4. Conclusions

This study presents a system-level analysis of a grid-connected PV–rSOC–MH microgrid with storage-constrained dispatch. The proposed dispatch strategy explicitly enforces hydrogen storage feasibility at each timestep, ensuring physically consistent operation. The system achieves a PV contribution of approximately 40% of the annual load, while grid imports account for about 60%, indicating significant grid dependency. Hydrogen production and consumption are balanced over the annual horizon (17,454 kg), confirming stable cyclic operation of the storage subsystem. The rSOC operates in SOEC, SOFC, and idle modes for approximately 11.5%, 6.6%, and 81.9% of the time, respectively, demonstrating its role as a long-duration balancing component. Exergy analysis identifies PV conversion as the dominant source of thermodynamic inefficiency (56.2%), followed by electrochemical losses in the rSOC and power electronics, while the contribution of hydrogen storage remains limited. These results indicate that improvements in PV efficiency and rSOC performance are critical for enhancing overall system performance. The results confirm that storage-constrained dispatch is essential to avoid infeasible operation in hydrogen-based microgrids and to ensure realistic system behavior under operational constraints. Future work will include degradation effects, dynamic operation, and techno-economic optimization.

Acknowledgments

The present work was carried out within the framework of the SOLID project, which received funding from the Cyprus Research and Innovation Foundation under the Cohesion Policy Programme “THALIA 2021–2027”, Grant Agreement No. BRIDGE2HORIZON/0823E/0210. The authors also acknowledge the PHAETHON Research and Innovation Centre of Excellence for Intelligent, Efficient and Sustainable Energy Solutions Horizon Europe Widespread Teaming project (https://teaming.phaethon-coe.eu/). The PHAETHON project has received funding from the European Union’s Horizon Europe Research and Innovation Programme under Grant Agreement No 101059898, from the Government of the Republic of Cyprus through the Deputy Ministry of Research and Innovation, and the University of Cyprus.

References

[1] Qi N., Huang K., Fan Z., Xu B., Long-term energy management for microgrid with hybrid hydrogen-battery energy storage: A prediction-free coordinated optimization framework. Applied Energy 2025;377:124485.

[2] Tariq A.H., Kazmi S.A.A., Hassan M., Ali S.A.M., Anwar M., Analysis of fuel cell integration with hybrid microgrid systems for clean energy: A comparative review. Int J Hydrogen Energy 2024;52:1005–1034.

[3] Arsalis A., Papanastasiou P., Georghiou G.E., Lifetime performance degradation of an anion exchange membrane electrolyzer under dynamic operation in a photovoltaic-powered nanogrid environment. Renewable Energy 2026;265:125615.

[4] Grigorovitch M., Vlad G., Nousdilis A., Kelepouris N., Arsalis A., Celli G., Mocci S., Christoforidis G., Georghiou G., Gal E., Integrated approaches to renewable energy: assessing the economic feasibility of PV, BESS, and DSM in Mediterranean public buildings. Energy Efficiency 2026;19:17.

[5] Arsalis A., Nousdilis A., Celli G., Bouhouras A., Christoforidis G., Mocci S., Georghiou G.E., Demand-side management in photovoltaic-battery microgrids: A multi-country assessment for Mediterranean public buildings. Energy & Buildings 2026;356:117111.

[6] Arsalis A., Nousdilis A., Celli G., Grigorovitch V., Bouhouras A., Christoforidis G., Mocci S., Grigorovitch M., Gal E., Georghiou G.E., Enhancing public building sustainability through integrated solar photovoltaic-based microgrid pilots: commissioning, operation, and performance insights. Renewable Energy 2026;262:125347.

[7] Arsalis A., Georghiou G.E., Papanastasiou P., Recent research progress in hybrid photovoltaic–regenerative hydrogen fuel cell microgrid systems. Energies 2022;15:3512.

[8] Maynard I., MacKay D., Schell K.R., Kilpatrick R., Abdulla A., Hydrogen microgrids to facilitate the clean energy transition in remote, northern communities. Applied Energy 2025;401:126758.

[9] Allwyn R.G., Margaret V., Al-Hinai A., Energy management of hybrid microgrids – A comparative study with hydroplus and methanol based fuel cells. Int J Hydrogen Energy 2024;85:909–930.

[10] Maciel L.B.B., Viola L., de Queiroz Lamas W., Silveira J.L., Environmental studies of green hydrogen production by electrolytic process: A comparison of the use of electricity from solar PV, wind energy, and hydroelectric plants. Int J Hydrogen Energy 2023;48:36584–36604.

[11] Zghaibeh M., Belgacem I.B., Barhoumi E.M., Baloch M.H., Chauhdary S.T., Kumar L., Arıcı M., Optimization of green hydrogen production in hydroelectric-photovoltaic grid connected power station. Int J Hydrogen Energy 2024;52:440–453.

[12] Huang C., Strbac G., Zong Y., You S., Træholt C., Brandon N., Wang J., Ameli H., Modeling and optimal operation of reversible solid oxide cells considering heat recovery and mode switching dynamics in microgrids. Applied Energy 2024;357:122477.

[13] Liu G., Kupecki J., Deng Z., Li X., Efficiency analysis of a novel reversible solid oxide cell system with the secondary utilization of the stack off-gas: A model-based study. J Clean Prod 2023;397:136570.

[14] del Pozo Gonzalez H., Bianchi F.D., Torrell M., Bernadet L., Eichman J., Tarancón A., Dominguez-Garcia J.L., Gomis-Bellmunt O., Predictive control for mode-switching of reversible solid oxide cells in microgrids based on hydrogen and electricity markets. Int J Hydrogen Energy 2025;102:120–128.

[15] del Pozo Gonzalez H., Bernadet L., Torrell M., Bianchi F.D., Tarancón A., Gomis-Bellmunt O., Dominguez-Garcia J.L., Power transition cycles of reversible solid oxide cells and its impacts on microgrids. Applied Energy 2023;352:121887.